ELSEVIER

Surface and Coatings Technology 158–159 (2002) 8–13

SURFACE & COATINGS TECHNOLOGY

www.elsevier.com/locate/surfcoat

Target material dependence of secondary electron images induced by focused ion beams☆

K. Ohya[a,*], T. Ishitani[b]

[a]*Faculty of Engineering, The University of Tokushima, Tokushima 770-8506, Japan*
[b]*Instruments Division, Hitachi High-Technologies Corp., Ichige, Hitachinaka, Ibaraki 312-8504, Japan*

Abstract

Monte Carlo calculation of ion-induced kinetic secondary electron emission was performed to study the target material dependence of secondary electron images in scanning ion microscopy (SIM) by using focused ion beams, which is different from that in scanning electron microscopy (SEM). In the calculation, the electron excitation by projectile ions is treated using the partial wave scattering cross-section of conduction electrons by the ions, and the cascade multiplication process of the excited electrons is simulated as well as the elastic collision cascade of recoiling target atoms. The calculated secondary electron yields of Al ($Z_2=13$), Cu ($Z_2=29$) and Au ($Z_2=79$) for 30 and 10 keV Ga^+ ion impacts decrease with increasing atomic number, Z_2, of the materials, whereas those for 1 keV H^+ ions and 10 keV electrons increase with Z_2. This is consistent with the observed opposite trend between the SIM and SEM in the Z_2 dependence of secondary electron images. Simultaneous calculation of individual elastic and inelastic collisions of the projectile ion, the recoiling target atoms and the excited electrons suggests that the Z_2 dependence of the secondary electron yield for heavy-ion impact is related to large elastic energy loss of the projectile ion and low energy of the excited electrons in the solid.

Keywords: Ion induced secondary electron emission; Monte Carlo simulation; Scanning ion microscopy; Focused ion beam; Material dependence

1. Introduction

In recent years, scanning ion microscopy (SIM) using focused ion beam (FIB) have demonstrated a unique imaging capability using the ion-induced secondary electron emission, which makes it an attractive complement to secondary electron microscopy (SEM) and secondary ion imaging [1]. However, it is well known that the material contrast of the secondary electron image produced by the FIB differs from that produced by the SEM. Of relevance to the secondary electron image is the dependence of the secondary electron yield on the atomic number, Z_2, of the target material. The information available to the Z_2 dependence is limited at present. The bombardment of metals by H^+, He^+, N^+, O^+, Ne^+ and Ar^+ ions yields a weak Z_2-dependence at 30 keV [2], whereas a strong Z_2-dependence exists for Ga^+ ion bombardment of metals. Furthermore, a recent experiment [3] has clearly shown that the brightness of the secondary electron images in the SIM decreases with increasing Z_2 for Al, Cu, Ag and Au, probably due to physical origin; while that in the SEM increases with Z_2.

The ion-induced secondary electron emission can be ascribed to the processes of potential emission and kinetic emission. The potential emission occurs due to the impact of ions with high ionization potential, such as noble gas ions, through the transfer of the potential energy to near-surface electrons before the ion hits the surface. The Ga^+ ion bombardment will not be subject to the potential emission because of its low ionization potential ($\sim$6.0 eV), according to Baragiola's empirical formula [2]. After it has hit the surface, the penetrating ion loses its energy due to elastic and inelastic collisions in the solid target. The energy transfer from the ions to the atoms due to the elastic collisions initiates cascade multiplication process of the recoiling solid atoms, leading to sputtering. The kinetic electron emission is

☆ Paper submitted to 12th International Conference on Surface Modification of Materials by Ion Beams, September 9–14, 2001, Marburg.

*Corresponding author. Tel. +81 886 56 7444; fax: +81 886 56 7444.

E-mail address: ohya@ee.tokushima-u.ac.jp (K. Ohya).

0257-8972/02/$ - see front matter © 2002 Elsevier Science B.V. All rights reserved.
PII: S0257-8972(02)00196-2

one of the most general consequences of the inelastic collisions of the ions in the solid. Electrons are excited as a result of the conversion of kinetic energy of the ions, the excited electrons undergo cascades of collisions in the solid, and some electrons escape into the vacuum before being thermalized, overcoming the surface potential barrier. Therefore, the kinetic secondary electron yield varies complicatedly with Z_2, due to the bulk and surface contributions. We have developed a Monte Carlo simulation code, which treats the bulk and surface processes of the moving particles (ions, atoms and electrons). The code allows us to calculate the energy and angular distributions of the particles, as well as the total particle yield emitted from the solid. This paper reports simulation calculations of secondary electron emission from Al ($Z_2=13$), Cu ($Z_2=29$) and Au ($Z_2=79$) for the impacts of 30 and 10 keV Ga^+ ions, 1 and 0.3 keV H^+ ions, and 10 and 1 keV electrons. The emphasis is placed on the target material dependence of the secondary electron yield, and then, the difference between the secondary electron images in the SIM and SEM.

2. Monte Carlo simulation code for ion-induced secondary electron emission

The basic concept of our Monte Carlo code is to simulate trajectories of projectile ions penetrating into a solid and of recoiling solid atoms and excited electrons traveling towards the solid surface with given mean-free-paths (MFPs) for elastic and inelastic collisions. The MFP for elastic collisions of projectile ions and recoil atoms with target atoms is assumed to be $\lambda_{el}=N^{-1/3}$, as chosen in many Monte Carlo codes for sputtering based on the binary collision approximation [4]; where N is the atomic density of the solid. Since one collision takes place in a cylinder of length λ_{el} and radius $(\lambda_{el}\pi N)^{-1/2}$, the actual impact parameter is randomly selected between 0 and $(\lambda_{el}\pi N)^{-1/2}$. The scattering angle is determined using the impact parameter according to a fast approximation procedure of atomic collisions in Ziegler–Biersack–Littmark interatomic potential, derived by Biersack and Haggmark [5].

The inverse MFP for electron excitation by various ions or atoms with velocity v is calculated using the partial wave expansion of scattering of a conduction electron by an ion or an atom [6], i.e.

$$\frac{1}{\lambda_{inel}}=\frac{3\pi n v}{4\sqrt{2}v_F^2}\sum_{l=0}^{\infty}\sum_{m=0}^{\infty}(2l+1)(2m+1)\times\{1-\cos2\delta_l(E_F)-\cos2\delta_m(E_F)+\cos[2(\delta_l(E_F)-\delta_m(E_F))]\}\times\int_{-1}^{1}(1-x)^{1/2}P_l(x)P_m(x)\mathrm{d}x$$

Here, $\delta_{l,m}$ is the phase shift for the scattering of the conduction electron at the Fermi energy E_F in the potential of the intruding ion or atom at rest, assuming the impact of slow ions ($v \ll v_0$, v_0: the Bohr velocity); $P_{l,m}$ and v_F are the Legendre polynomials and the Fermi velocity, respectively. n is the density of homogeneous electron gas, which is related to a radius, r_s, of a sphere that contains one electron, i.e. $n=3/(4\pi r_s^3)$; in this calculation, $r_s=2.12$, 1.83 and 1.49 in units of the Bohr radius for Al, Cu and Au, respectively [7]. The phase shifts are calculated by solving the radial wave equations for each partial wave with the bound atom potential obtained by Salvat and Parellada [8].

The motions of projectile ions and recoil atoms in the solid are treated in the same way; the step length L is determined from the total MFP, λ_T, defined as $1/\lambda_T=1/\lambda_{el}+1/\lambda_{inel}$, i.e. $L=-\lambda_T\ln R$, where R is a random number. Depending on each of the inverse MFPs, $1/\lambda_{el}$ and $1/\lambda_{inel}$, either the elastic or inelastic collision is chosen by using another random number. If the elastic collision is chosen, the scattering angle and the elastic energy loss are calculated; the particle changes its direction of motion and loses its energy discretely. In each elastic collision process, a new recoil atom is generated, and then, a recoil collision cascade is simulated. The displacement energy, which the recoil atom has to receive in order to leave its lattice site, is ignored. If the inelastic collision is chosen, the particle loses its energy, taking its directional change into account, and liberates an electron. The energy of liberated electrons is equal to the energy loss of the particle due to the inelastic collision, i.e. $\Delta E=2m_e[v_i+(v_F/2)]^2$, which is calculated from a head-on collision of the particle with the Fermi electron [9]. The initial directional angle of the electron is calculated using the energy and momentum conservation law according to the classical collision scheme.

The liberated electrons interact with the solid through elastic collisions with the solid atoms, and through inelastic collisions, i.e. excitations of conduction electrons, bulk plasmons, including their successive decay with excitation of conduction electrons, and inner-shell electrons, e.g. 2p- and 2s-shells for Al. The MFPs for excitations of the conduction electrons and bulk plasmons are calculated according to Tung and Ritchie [10], whereas for excitation of the inner-shell electrons the MFP (the cross-section) is taken from Gryzinski [11]. The elastic MFP is calculated using the screened Rutherford formula where the screening parameter is determined as a function of the electron energy according to Fitting and Reinhardt [12]. According to the Monte Carlo method, the trajectory of each electron is chosen using a series of random numbers to determine the path length between collision events, the type of collision that takes place and the energy loss or scattering angle. In each inelastic process, secondary electrons are excited, and as a result, electron cascades are generated. The

electron cascade model is applied to the secondary electron emission under electron bombardment [13].

The projectile ion, the recoil atoms, and the excited and the cascade electrons are followed until their energy falls below the surface binding energy E_s and the surface potential energy $E_F+\Phi$ (Φ: the work function), respectively, or until they overcome the surface and escape into the vacuum. The values of E_s, E_F and Φ used here are as follows [14–16]: for Al, $E_s=3.36$ eV, $E_F=11.65$ eV and $\Phi=4.28$ eV; for Cu, $E_s=3.52$ eV, $E_F=7.03$ eV and $\Phi=4.65$ eV; for Au, $E_s=3.80$ eV, $E_F=5.52$ eV and $\Phi=5.10$ eV. Since the planar surface barrier model [17] is adopted, the particles are emitted with reduced energy in a refracted direction due to the surface binding energy or the surface potential barrier. In each of the Monte Carlo calculations conducted here, the electrons and recoil atoms are generated by normal incidence of 10^4 ions.

3. Numerical results and discussion

The ion-induced kinetic secondary electron emission occurs if the projectile ion transfers sufficient kinetic energy to the conduction electrons to overcome the surface potential barrier, so that the kinetic secondary electron emission is subject to an impact energy threshold. To a first approximation, the threshold energy is conventionally calculated from the condition that the energy transfer from a projectile ion in a head-on collision with a nearly free conduction electron is equal to the surface work function: $E_{th}=(1/2)m_p v_{th}^2$ and $v_{th}=(1/2)v_F[(1+\phi/E_F)^{1/2}-1]$, where m_p is the projectile mass [18]. Thus, for Al, Cu and Au, the threshold energies per ion mass unit are approximately 154, 270 and 381 eV/amu, respectively; the heavier both the ion and the target atom are, the higher is the threshold energy. For the impacts of Ga^+ ions (69.7 amu), however, extremely high threshold energies are estimated: 10.7, 18.8 and 26.6 keV, respectively. This indicates that no secondary electron is emitted by 10 keV Ga^+ ions and very small yield of secondary electrons is expected for 30 keV Ga^+ ions. On the other hand, some experimental observations for the impacts of heavy ions, e.g. Ar^+ and Xe^+ ions, on clean polycrystalline Au [19,20] have revealed a considerably smaller threshold energy (10 eV/amu) than the conventional value and an electron yield of 0.08, which is much larger than the potential electron yield ($\sim$0.02), for 3 keV Ar^+ ions [19]. In the case of Ga^+ ions, few direct excitation of conduction electrons by recoil atoms will contribute to the total secondary electron yield, because the energy of the recoil atoms is much lower than that of the projectile ions: the average energy is 238, 419 and 314 eV for the impacts of 30 keV Ga^+ ions on Al, Cu and Au, respectively. One of the electron emission mechanisms below the conventional threshold is the promotion

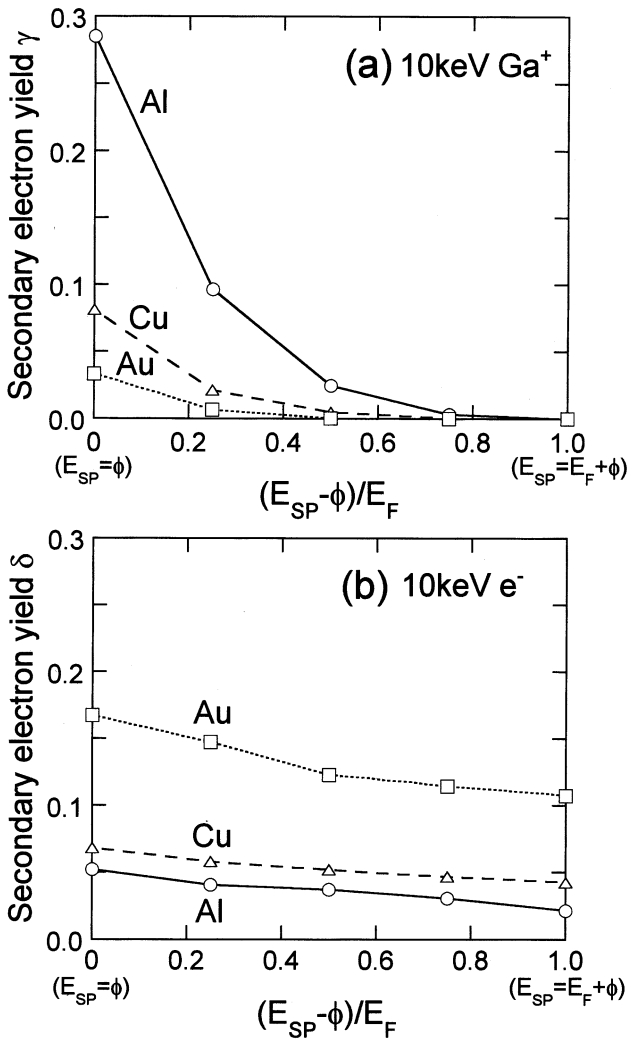

Fig. 1. Secondary electron yields, γ and δ, of Al, Cu and Au for the impacts of (a) Ga^+ ions and (b) electrons, respectively, with the energy of 10 keV, as a function of apparent surface potential barrier, E_{sp}.

of core electrons into the vacuum or the conduction band due to internal Auger process [21] or quasi-molecule formation [22,23]. The mechanism increases the number of electrons in the high energy levels in the conduction band, which decreases the apparent surface potential barrier for the excited electrons. In this study, therefore, the surface potential barrier, E_{sp}, for the impact of Ga^+ ions is taken between $E_F+\phi$ (emission from the bottom of the conduction band) and ϕ (emission from the top of the conduction band).

Fig. 1 shows the calculated secondary electron yield of Al, Cu and Au impacted by 10 keV Ga^+ ions and 10 keV electrons, as a function of the apparent surface potential barrier. The secondary electron yield for Ga^+ ions substantially increases due to the lowering in the surface potential barrier, whereas for electrons it less increases. When $E_{sp}=\phi$, furthermore, the secondary electron yields of Al and Cu for 10 keV Ga^+ ions are

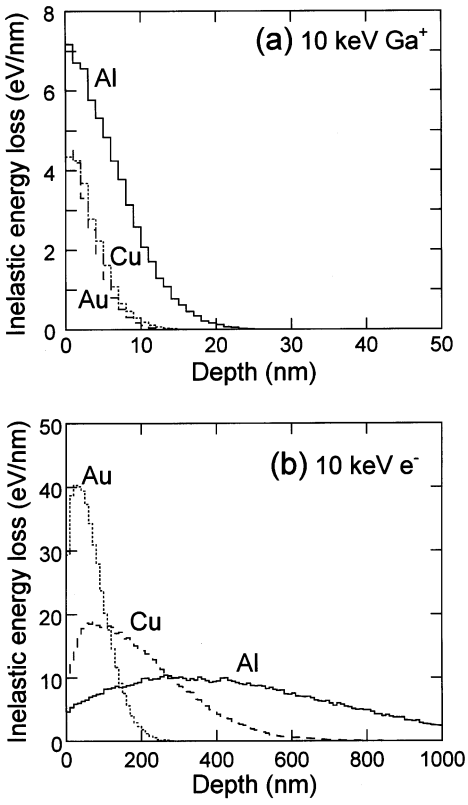

Fig. 2. Depth distributions of inelastic energy loss of (a) Ga^+ ions and (b) electrons in Al, Cu and Au at the impact energy of 10 keV.

larger than the values for 10 keV electrons, whereas for $E_{sp}=E_F+\phi$, no secondary electrons are emitted. These are due to shallow excitation of electrons by Ga^+ ions (Fig. 2) and low energy of the excited electrons (Fig. 3). However, it should be noted that the order of the calculated secondary electron yields for both Ga^+ ions

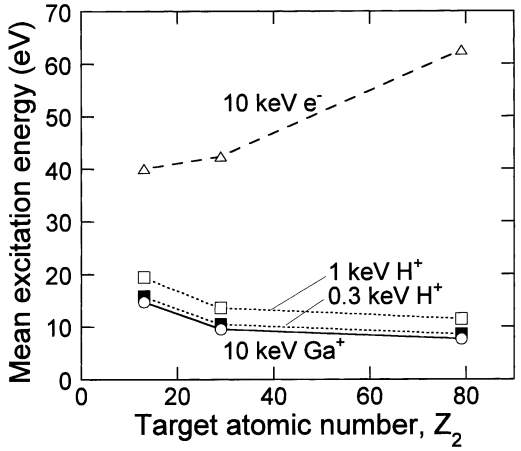

Fig. 3. Mean energies of excited electrons in Al ($Z_2=13$), Cu ($Z_2=29$) and Au ($Z_2=79$) due to the impacts of 10 keV Ga^+ ions, 10 keV electrons, and 1 keV and 0.3 keV H^+ ions, as a function of the atomic number, Z_2, of the target metals.

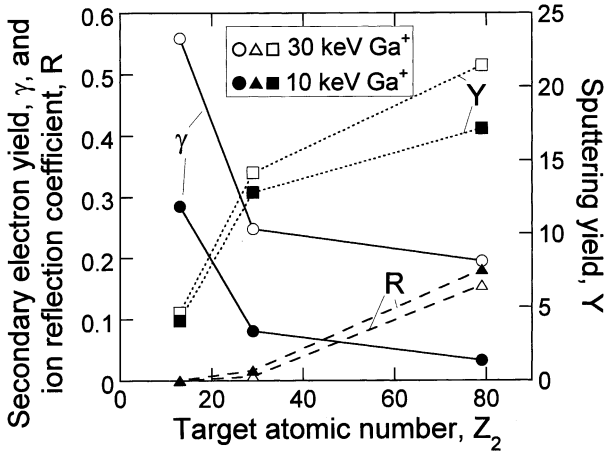

Fig. 4. Secondary electron yield, γ, ion reflection coefficient, R, and sputtering yield, Y, of Al ($Z_2=13$), Cu ($Z_2=29$) and Au ($Z_2=79$) due to the impacts of 30 and 10 keV Ga^+ ions, as a function of the atomic number, Z_2, of the target metals.

and electrons as a function of the atomic number, Z_2, of the materials is independent of the change in the surface potential barrier between $E_F+\phi$ and ϕ.

In Figs. 4 and 5, the secondary electron yields for the impacts of 30 and 10 keV Ga^+ ions, and 10 and 1 keV electrons, respectively, are shown as a function of the

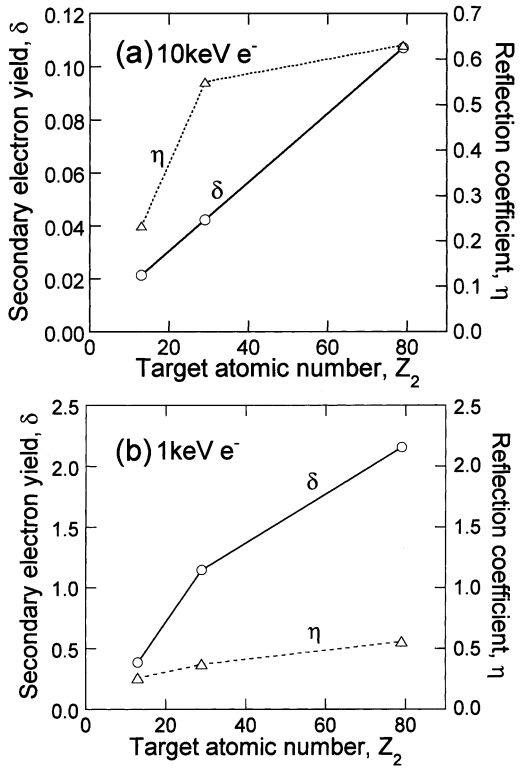

Fig. 5. Secondary electron yield, δ, and electron reflection coefficient, η, of Al ($Z_2=13$), Cu ($Z_2=29$) and Au ($Z_2=79$) due to the impacts of (a) 10 keV and (b) 1 keV electrons, as a function of the atomic number, Z_2, of the target metals.

atomic number, Z_2, of the materials. There is clearly different Z_2 dependence between Ga^+ ions and electrons; in the calculation, $E_{sp}=\phi$ and $E_{sp}=E_F+\phi$ for Ga^+ ions and electrons, respectively. The secondary electron yield depends on the number of excited electrons and the fraction of the electrons reaching the surface with enough energy to overcome the surface potential barrier; the former is closely related to the inelastic energy loss of the projectile particle in the solid. The reflection of the projectile particles from the surface decreases the secondary electron yield for two reasons; one is the decrease in the traveling path where the particles excite electrons, and the other is the reflection immediately after incidence without exciting electrons. Large reflection coefficients of heavy metals for projectile electrons results in the decrease in the secondary electron yield. For the impact of 10 and 1 keV electrons, however, the large increase in the secondary electron yield with increasing Z_2 is calculated due to the strong decrease in the penetration depth (or projected range) of projectile electrons, which results in frequent excitation of electrons near the surface, as shown for 10 keV electrons in Fig. 2. On the other hand, the electron excitation by Ga^+ ions is localized in the near-surface layer of less than 20 nm where the excited electrons are easy to escape from the surface. Therefore, the strong decrease in the secondary electron yield for Ga^+ ions with increasing Z_2 is due to both the decrease in the number of electron excitation events and the lowering in the energy of the excited electrons. For the impact energy of 10 keV, the mean energy of electrons excited during the penetration of Ga^+ ions into the solid is approximately 10 eV, which decreases with increasing Z_2 and is much smaller than that for electron impact (Fig. 3). The lowering in the excitation energy limits the number of electrons to overcome the surface potential barrier and be emitted into the vacuum. Furthermore, the low excitation energy comparable to the surface potential energy results in the high projectile energy for the conventional threshold of kinetic secondary electron emission.

For the impact of Ga^+ ions (Fig. 4), there are much larger sputtering yields and smaller reflection coefficient in comparison with light (H^+) ions (Fig. 6a). These are due to, by one or two orders of magnitude, larger elastic energy loss of the heavy ions, which increases with increasing Z_2 of the materials. The large elastic energy loss causes the penetrating ions to lose their energy quickly. Since the energy of excited electrons, ΔE, decreases with decreasing ion energy (or velocity v_i), the large energy loss of the ions in their traveling path results in the lowering in the energy of excited electrons. Therefore, the secondary electron yield for Ga^+ ions decreases with increasing Z_2, whereas the sputtering yield increases; the reflection coefficients of Ga^+ ions

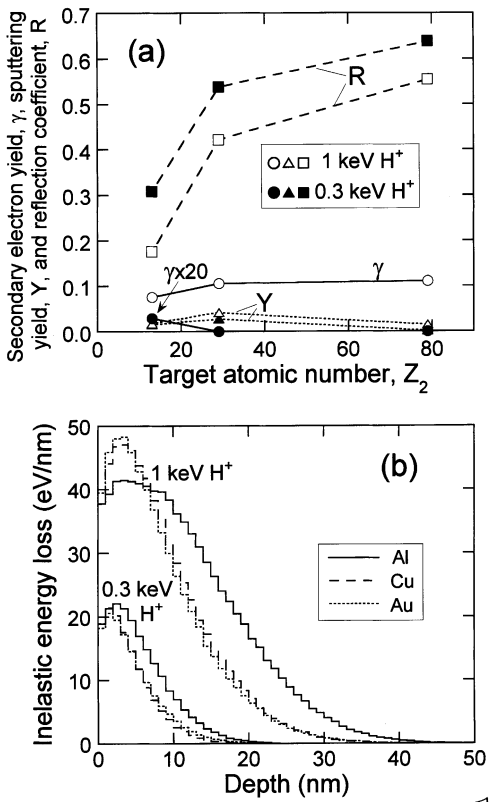

Fig. 6. (a) Secondary electron yield, γ, ion reflection coefficient, *R*, and sputtering yield, *Y*, of Al ($Z_2=13$), Cu ($Z_2=29$) and Au ($Z_2=79$) due to the impacts of 1 and 0.3 keV H^+ ions, as a function of the atomic number, Z_2, of the target metals. (b) The depth distribution of inelastic energy loss of 1 and 0.3 keV H^+ ions in the same species of the target materials as (a).

is much smaller than those for the light (H^+) ions and electrons.

For the impact of light ions, such as H^+, the secondary electron yield shows rather weak dependence on Z_2, as shown in Fig. 6a. Except for low energy (<1 keV), the projectile H^+ ions lose their energy mainly due to the electron excitation (i.e. inelastic energy loss) and the ion range is larger than the escape depth of excited electrons, in the same way as the case of the electron impact (Fig. 2b). In comparison to Fig. 6b with Fig. 2b, however, the depth distribution of the inelastic energy loss of H^+ ions does not clearly change due to change in Z_2, so that the secondary electron yield shows weak dependence on Z_2.

For very low energy (0.3 keV) approaching the conventional threshold, where the inelastic energy loss of H^+ ions is comparable to the elastic energy loss, the calculated secondary electron yield for H^+ ions decreases with increasing Z_2, due to the increase (decrease) in the elastic (inelastic) energy loss of the projectile ions. In addition to the low energy of excited electrons (Fig. 3), the Z_2 dependence will be caused by the increase in

the reflected projectiles due to the large reflection coefficient for H^+ ions.

4. Conclusions

The atomic number (Z_2) dependence of secondary electron images in the SIM, which is different from that in the SEM, was investigated by Monte Carlo simulations for ion-induced and electron-induced secondary electron emission. The Monte Carlo code simulates trajectories of projectile ions penetrating into a solid and of recoiling solid atoms and excited electrons traveling towards the solid surface with given mean-free-paths (MFPs) for elastic and inelastic collisions. The calculated secondary electron yields of Al ($Z_2=13$), Cu ($Z_2=29$) and Au ($Z_2=79$) for 30 and 10 keV Ga^+ ion impacts decrease with increasing Z_2, whereas those for 10 and 1 keV electrons and 1 keV H^+ ions increase. The observed opposite trend between the SIM and SEM in the Z_2 dependence was simulated by our Monte Carlo calculation for the first time. Simultaneous calculation of individual elastic and inelastic collision processes of the projectile ion, the recoiling target atoms and the excited electrons revealed that the Z_2 dependence of the secondary electron yield is related to the elastic energy loss of the projectile ion, the electron excitation cross-section and the energy of excited electrons in the solid.

As observed for 27 species of metals with H^+, He^+ and Ar^+ ions at high energies ($\geqq$100 keV) by Hasselkamp et al. [24], however, the detailed periodic structure will be superimposed on the monotonous change in the secondary electron yield with three target materials used for calculation. Furthermore, the periodic changes in the secondary electron yield of 30 species of metals for the impacts of 10 keV electrons and 3 keV Ar^+ ions were measured, which indicates an interesting oscillations of the secondary electron yields in opposite phases between Ar^+ ions and electrons [25]. Therefore, detailed studies of the Z_2 dependence, including the periodic structure, of the secondary electron yield will be done with further calculation and discussion with more target species.

References

[1] R. Levi-Setti, Scanning Electron Microscopy/, SEM Inc, Chicago, 1983, p. 1.
[2] R.A. Baragiola, E.V. Alonso, J. Ferron, A. Oliva-Florio, Surf. Sci. 90 (1979) 240.
[3] Y. Sakai, T. Yamada, T. Suzuki, T. Sato, H. Itoh, T. Ichinokawa, Appl. Phys. Lett. 73 (1998) 611.
[4] W. Eckstein, Computer Simulation of Ion–Solid Interactions, Springer, Berlin, 1991, p. 83.
[5] J.P. Biersack, L.G. Haggmark, Nucl. Instrum. Meth. 174 (1980) 257.
[6] J.C. Ashley, A. Gras-Marti, P.M. Echenique, Phys. Rev. A 34 (1986) 2495.
[7] J.F. Ziegler, J.P. Biersack, U. Littmark, The Stopping and Range of Ions in Solids, Pergamon, New York, 1985, p. 264.
[8] F. Salvat, J. Parellada, J. Phys. D 17 (1984) 1545.
[9] M. Rösler, in: R. Baragiola (Ed.), Ionization of Solids by Heavy Particles, Plenum, New York, 1993, p. 27.
[10] C.J. Tung, R.H. Ritchie, Phys. Rev. B 16 (1977) 4302.
[11] M. Gryzinski, Phys. Rev. A 138 (1965) 336.
[12] H.J. Fitting, J. Reinhardt, Phys. Status Solidi A 88 (1985) 245.
[13] K. Ohya, J. Kawata, Scanning Microsc. 9 (1995) 331.
[14] W. Eckstein, Computer Simulation of Ion-Solid Interactions, Springer, Berlin, 1991, p. 73.
[15] C. Kittel, Introduction to Solid State Physics, 6th ed., John Wiley & Sons, New York, 1986, p. 248.
[16] D.R. Lide (Ed.), Handbook of Chemistry and Physics, 74th ed., CRC, Boca Raton, 1993, pp. 12–105.
[17] T. Koshikawa, R. Shimizu, J. Phys. D: Appl. Phys. 7 (1974) 1303.
[18] R.A. Baragiola, E.V. Alonso, A. Oliva-Florio, Phys. Rev. B 19 (1979) 121.
[19] K. Töglhofer, F. Aumayr, H.P. Winter, Surf. Sci. 281 (1993) 143.
[20] E.V. Alonso, M.A. Alurrade, R.A. Baragiola, Surf. Sci. 166 (1986) L155.
[21] E.S. Parilis, L.M. Kishinevskii, Sov. Phys. Solid State 3 (1960) 885.
[22] P. Joyes, Radiat. Effects 19 (1973) 235.
[23] H.P. Winter, H. Eder, F. Aumayr, Int. J. Mass. Spectrom. 192 (1999) 407.
[24] D. Hasselkamp, S. Hippler, A. Scharmann, T. Schmehl, Ann. Phys. 47 (1990) 555.
[25] M. Kudo, Y. Sakai, T. Ichinokawa, Appl. Phys. Lett. 76 (2000) 3475.